

STATE OF THE ART IN COMPUTATIONAL ANALYSIS OF CAVITATION INCEPTION AND ITS SCALE EFFECTS

Reference NO. IJME 814, DOI: 10.5750/ijme.v164iA4.814

E L Amromin, Mechmath Limited Liability Company, USA

KEY DATES: Submitted: 29/11/21; Final acceptance: 22/02/23; Published: 27/03/23

SUMMARY

Mathematical analysis of cavitation inception is an important topic for naval engineering, but several circumstances make it difficult. First, cavitating flows are substantially multi-zone flows, where the appearing cavities are incomparably smaller than a cavitating body is. Second, inception is substantially influenced by the characteristics of the inflow and of the body surfaces. Third, validation of employed mathematical methods by comparison with experimental data is a non-trivial task because of the complexity of experiments themselves and scale effects. This paper is emphasized on multi-zone quasi-steady approaches for prediction of cavitation inception and desinence numbers. The obtained computational results are compared with the known experimental data for sheet cavitation, vortex cavitation and cavitation behind surface irregularities. Procedures for scaling of cavitation inception number and the eventual combinations of various CFD solvers are also discussed.

NOMENCLATURE

C	Hydrofoil chord
C_p	Pressure coefficient
D	Body diameter (m)
H	Size of roughness element (m)
N	Normal to the flow boundaries
N_x	Component of N
P_0	Ambient pressure (Pa)
P_c	Pressure in cavity (Pa)
\tilde{p}	Pressure pulsation (Pa)
R	Radius of vortex viscous core (m)
R_c	Radius of a bubble (m)
Re	Reynolds number
U_0	Inflow speed (m/s)
U	Dimensionless water velocity
$\langle u'v' \rangle$	Reynolds stress (m^2/s^2)
\dot{V}	Variation of the cavity volume (m^3)
v^*	Friction velocity (m/s)
w	Circumferential velocity (m/s)
X_1, X_2	Abscissas of the cavity edges
y_0	Ordinate of "a virtual wall" (m)
Γ	Vortex intensity (m^2/s)
a	Inflow air content
δ	Boundary layer thickness (m)
δ^*	Thickness displacement (m)
χ	Surface tension coefficient (H/m)
σ	Cavitation number
σ_D	Cavitation desinence number
σ_I	Cavitation inception number
σ_{vapor}	Vapour cavitation number
ρ_w	Density of water (kg/m^3)
ν	Water kinematic viscosity (m^2/s)

1. INTRODUCTION

The main incentive for studies of cavitation inception has been the accompanying jump of flow-induced noise

(illustrated here by Figure 1 with the data from the Blake's (1986) book). Prediction of cavitation inception in marine engineering has been associated with the necessity to predict the silence operation speeds for military vehicles (an interest to the environmental impact of such a jump appeared more recently). Determination of such a speed has been traditionally based on the model tests in hydrodynamic facilities (mainly in water tunnels) with the similarity criterion $\sigma = 2(P_0 - P_c) \rho_w^{-1} U_0^{-2}$. Usually, the test results must undergo an extrapolation to the ranges of Reynolds numbers that are much greater than the model test values of Re .

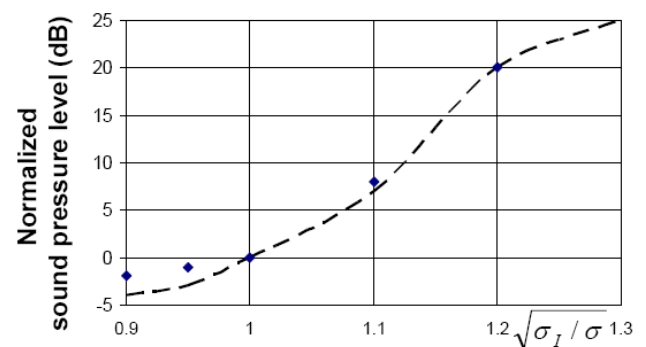


Figure 1. Noise of two propellers. Rhombi and dashed curve relate to different propellers.

Meanwhile, the earliest reviews on cavitation inception published by Lindgren and Johnson (1966) and by Acosta and Parkin (1975) manifested that even for the same body there is no a general trend $\sigma_i(Re)$ for cavitation inception number σ_i (for the value of σ corresponding to appearing/disappearing cavitation). Some data from the first of these reviews are shown in Figure 2 to support the above sentence. No computational analysis of such experiments

appeared at the time of these reviews. One can recall the pessimistic tone of Birkhoff's (1971) review of the state-of-the art in mathematical analysis of cavitation published at that time. Cavitating flows have been studied then exclusively in the framework of ideal fluid theory. Moreover, the main mathematical tool has been inversion of variables with the following use of some hodograph planes. Such a tool works well for bodies of simple shapes (like flat plate, wedges, etc.). However, as shown in Figure 3, even for a hydrofoil the image of its wetted part in a hodograph plane is very complex. Therefore, it was too difficult to find the corresponding conform mapping.

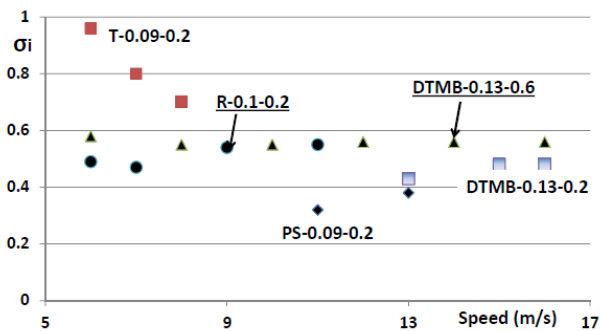


Figure 2. Vapour cavitation inception number for bodies with hemispherical heads. Symbols marked as T-0.09-0.2 show data for the body of diameter $D=0.09\text{m}$ in Tokyo water tunnel with air content 0.2 of saturation, similarly marked symbols R show data for Rome water tunnel, PS show data for Penn State water tunnel, DTMB for David Taylor Model Bassin water tunnel.

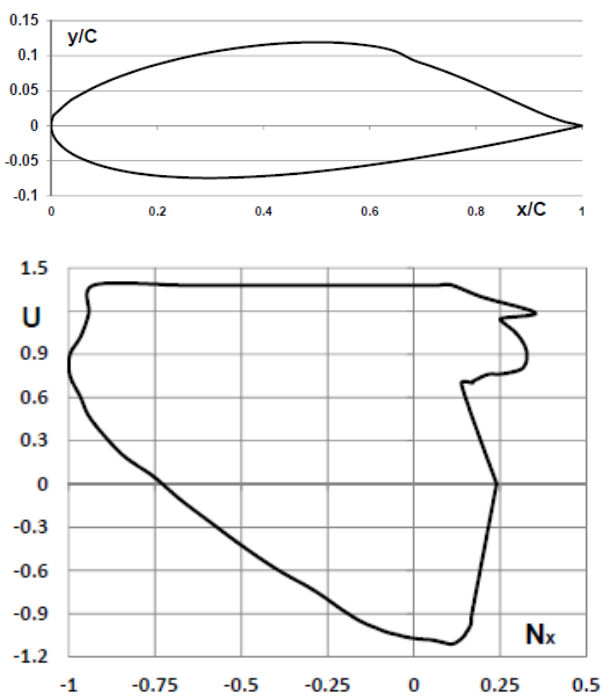


Figure 3. Flow boundaries around cavitating foil OK2003 in planes $\{x, y\}$ and $\{U, N_x\}$.

The following decades have been distinguished by the noticeable successes in the development of computational tools for cavitating flows. Now there The following decades have been distinguished by the noticeable successes in the development of computational tools for cavitating flows. Now there are two major groups of such tools applicable to marine engineering. One group is based on the iterative methods for nonlinear free-surface problems of ideal fluid described by Ivanov (1980), Uhlman (1987), Pelone and Rowe (1988). This group also allows for employment in viscous-inviscid interaction procedures with implementation of the multi-zone model (MZM) considering sheet cavitation as a specific kind of viscous separation. Another group is based on employment of solvers for fully turbulent flows described by Kunz *et al* (2000), Ahuja *et al* (2001), Singhal *et al* (2002), Coutier-Delgosha *et al* (2007). This group considers flows of a single medium of the variable density (MVD) instead of flows of a liquid with cavities of certain borders. The advantage of the contemporary solvers of this group is the possibility to obtained computational results for various 3D body shapes. Both groups have been employed in the attempts to predict cavitation inception.

Though recently the spectrum of scientific interest to cavitation inception is not limited by maritime applications (as one can find in the review by Caupin and Herbert (2006), this happened even for water flows) this paper is limited by them. Moreover, only studies emphasized on determination of cavitation inception number (silent operation speed) will be considered here.

2. EXPLANATION OF DEFINITIONS

Paradoxically two substantial issues related to mathematical analysis of cavitation inception are the issues of definitions. The first issue is the definition of cavitation number. The majority of experimental results were presented with employment of vapour cavitation number σ_{vapor} calculated using vapour pressure instead of the actual pressure in the cavity. This replacement takes place because the actual pressure is difficult to measure. However, as shown in Figure 4 with the data of Arndt and Keller (1992) for the hydrofoils NACA4412, Kopriva *et al* (2008) for the hydrofoil OK2003, Wade and Acosta (1966) for a convex hydrofoil, Ganesh *et al* (2016) for a wedge, the ratio $\sigma_{\text{vapor}}/\sigma$ is significantly differs from 1.0.

The second issue is in the diverse definitions of cavitation inception. The oldest of them consists of observation of smallest cavities. There are two methods to find such a cavity in experiments. The first one is based on a gradual decrease of σ in cavitation-free flows. This method provides just cavitation inception number, but the inception phenomenon is quite random, the discrepancy of σ_1 is relatively high and often observation of the smallest cavity is difficult because its location can be initially unknown. The second one is based on a gradual increase of

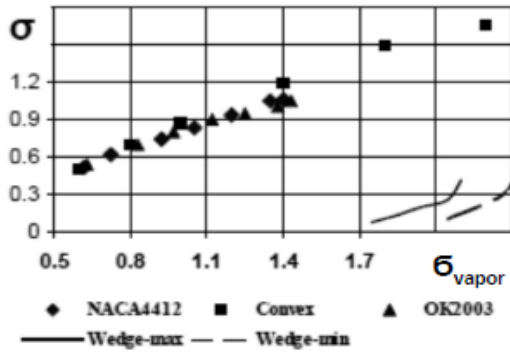


Figure 4. Cavitation number versus vapour cavitation number for various models.

σ in cavitating flows. Disappearance of the existing cavity allows for determination of cavitation desinence number. Its values have a lower discrepancy (as seen in Figure 5 with Katz (1984) data). Also, it is easier to observe the cavity collapse at its known location. The second method has been used in the majority of known experiments and most frequently just the values of σ_D have been reported as cavitation inception numbers. Nevertheless, there is the uncertainty in the definition of σ_D caused by impact of the size of disappearing cavity on the values of σ_D . This impact (illustrated by Figure 6 copied from Amromin's (2016) paper) complicates validation of numerical results because information on the cavity size corresponding to its desinence usually absents in published papers.

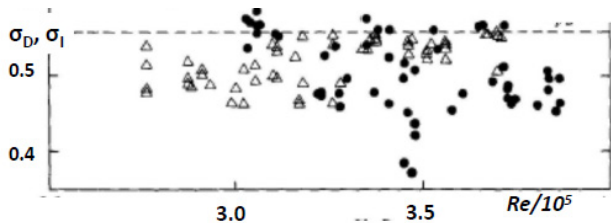


Figure 5. Observed cavitation inception (circles) and desinence (triangles) numbers for a body with hemispherical head.

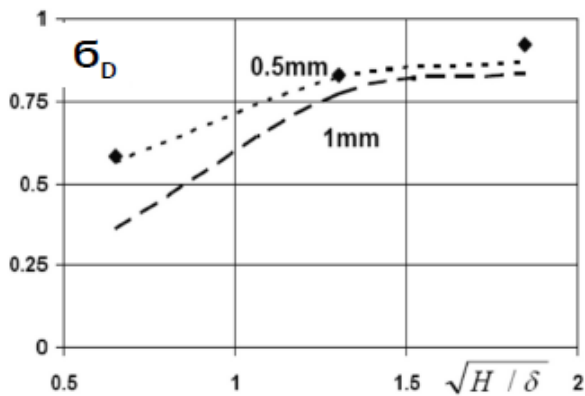


Figure 6. Impact of cavity size (shown at the curves) on computed cavitation desinence numbers for ridges in flows without pressure gradient; rhombi – experimental data. Numbers at curves show the cavity size.

Besides, because of the effect of surface tension, a smallest cavity may exist not at the greatest cavitation number. An example of such a situation with Amromin (2021) computations and measurements of Ceccio and Brennen (1992) is provided in Figure 7. The decreasing computed dependency $X_2(\sigma) - X_1(\sigma)$ relates to cavitation desinence, the increasing dependency relates to its inception.

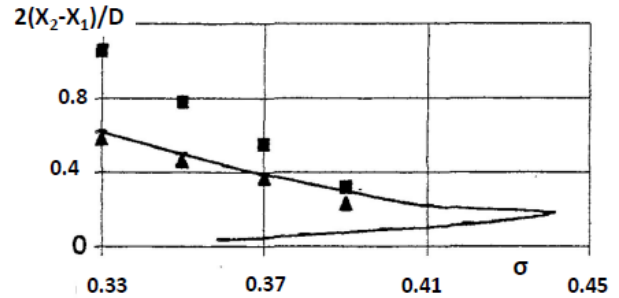


Figure 7. Squares and triangles show maxima and minima of observed cavity length over a body with hemispherical head, lines show its computed time-average value.

Another definition of inception is associated with counting of the inception events (as described by Waniewski and Brennen (1999), f. e.). However, it is difficult to distinguish the smallest cavities from the cavitation nucleus and no link between the number of events and σ_i was suggested. There is also a possibility to detect inception acoustically because the jump of flow-induced noise is directly proportional to variations of the cavity volume \dot{V} because $\dot{p} \sim d^2 \dot{V} / dt^2$. However, as pointed out by Vrijdag (2009), “studies on the systematic difference between the acoustic and the visual inception bucket have never been published in the public domain”.

In the computational results presented in this paper cavitation inception will be defined by the maximum value of σ in cavitating flows. This definition corresponds to the experimental determination of σ_D .

3. STUDY OF SHEET CAVITATION

Cavitation can appear in various forms. Sometimes it starts in the form of traveling bubbles, but more frequently the cavities appear at the body surface (as sheet cavitation) or within big vortices near it. As discovered by Arakeri (1975), sheet cavitation is a special kind of viscous separation. The scheme of flow invented for its analysis by Amromin (1985) and employed in his MZM computations is shown in Figure 8. A comparison of pressure distributions in cavitating flows of ideal fluid (ideal cavity) and of viscous fluid is given in Figure 9. One can see there that in viscous fluid the pressure minimum takes place upstream of the cavity (not at the cavity boundary, as was accepted a half century ago). For the same cavitation number, the ideal fluid theory predicts larger cavities. As was shown by Pelone and Rowe (1988), shape of these cavities substantially depends on X_1 . However, X_1 cannot be determined by that theory.

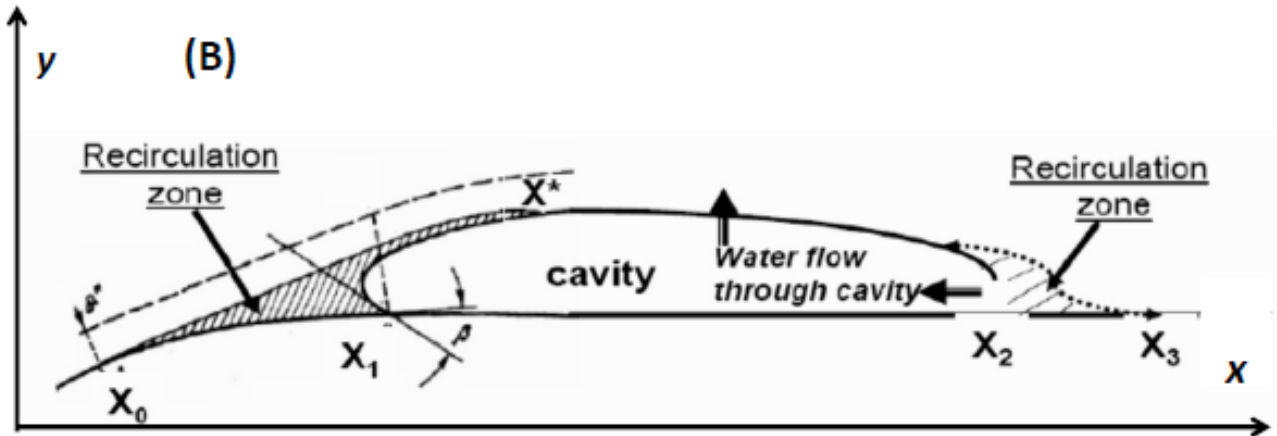


Figure 8. Scheme of meridian section of the cavity and its vicinity; boundary layer separates from the body surface at $x=X_0$ and reattaches to the cavity surface at $x=X^*$; further this layer separates from the cavity trailing edge at $x=X_2$ and reattaches to the body at $x=X_3$; $x=X_1$ is the cavity detachment point. Meridian sections of S are shown by dashed lines.

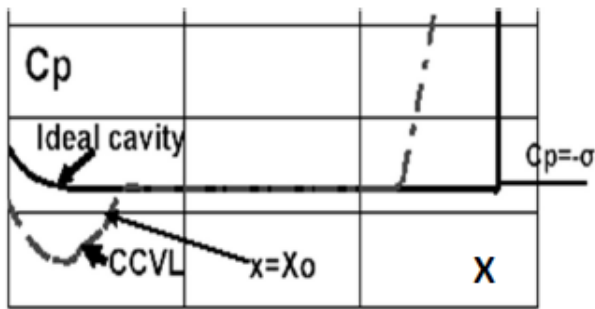


Figure 9. Comparison of pressure distributions around the cavity in cavitating flows of ideal and of viscous fluid (CCVL line).

The presented MZM results on cavitation inception were obtained with employment of a viscous-inviscid interaction procedure. Let us remind that this procedure divides the entire flow into a viscous part and an inviscid part with an initially unknown boundary between them. Their interaction is based on two effects. First one is the influences of pressure gradient on thicknesses of boundary layers. Second one is pressure variation as a result of variation of this thickness. Such a mutual influence requires iterations in the solving procedures.

In 2D or axisymmetric problems on sheet cavitation, it is convenient to order the cavity edges X_1 , X_2 and Re . The intermediate flow characteristics (in particular, the edges of viscous separation zones surrounding the cavity), the cavity shape, the corresponding values of σ and D (or C) can be determined in iterations using BEM for the inviscid flow and integral relationships for the viscous flow in turns, as made by Amromin (1985, 2014, 2021). The important feature of these relationships is employment of the special velocity profiles across recirculation (separation) zones; these profiles are adjusted to the existence of reverse flow in these zones and to the absence of logarithmic sub-layers there (unlikely to known MVD solvers (as one can see

from the data of Gonsales and Patella (2009) in Figure 10). Recently Zhang *et al* (2020) presented more results on dissimilarity of velocity profiles in cavitating and cavitation-free flows.

Computation of boundary layers in MZM starts from laminar boundary layers and transition. There is no continuity of velocity profiles from one zone to another, but the mass and momentum conservation laws across the viscous part of the flow are kept. The boundary between inviscid and viscous parts of flow over separation zones is a free boundary which shape depends on the pressure profiles along them. The pressure profiles are adjusted to the criteria of boundary layer separation and reattachment. These criteria include semi-empirical coefficients (on the other hand, the numerical tools of one-zone RANS and LES models operate with much more complex equations that include numerous empirical coefficients; in particular, the simplest RANS Spalart-Allmaras model for the attached turbulent flows uses at least 17 empirical and tuning coefficients). The distance from the free boundary to the body surface over the attached boundary layer equals to δ^* .

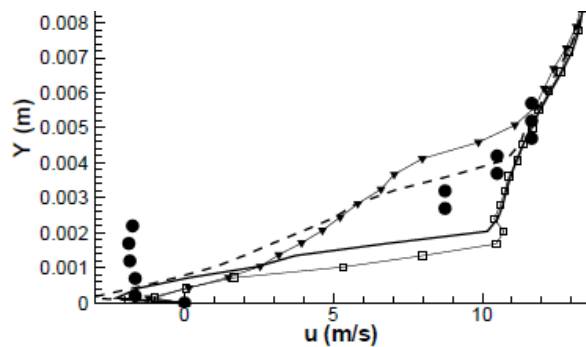


Figure 10. Comparison of measured (circles) and computed using MVD (lines) velocity profiles across a section of the cavity; diverse lines correspond to the diverse assumptions on the cavity content (sound speed in two-phase medium inside the cavity); $Re=2.7 \cdot 10^6$.

A comparison of cavitation inception and desinence numbers for hydrofoil CAV2003 computed using MZM and MVD with the experimental data is given in Figure 11. It is necessary to point out that the presented MVD results of Coutier-Delgosha *et al* (2007) are the best results on cavitation inception or desinence obtained using MVD models. One can see that both models provide the close values of σ_D . These values are within the discrepancy of experimental data. However, MZM provides the much more accurate cavity location (the smallest computed cavities are compared in Figure 12). So, consideration of diverse flow zones appears to be more important than a more detailed description of the flow in each zone.

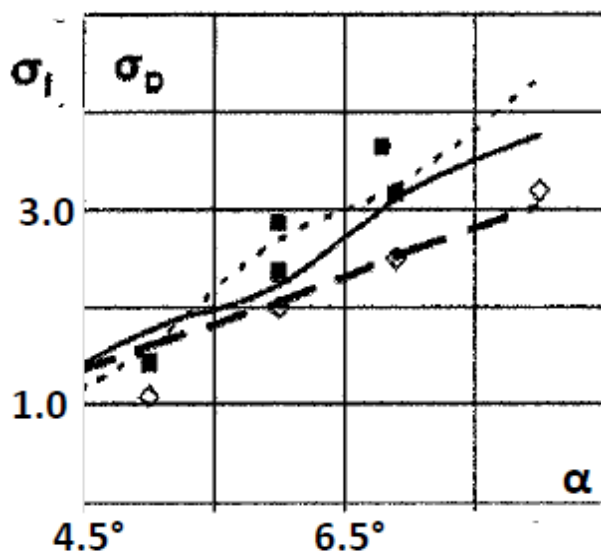


Figure 11. Cavitation inception and desinence numbers for hydrofoil CAV2003 versus its angle of attack; dotted lines show σ_D computed by Coutier-Delgosha *et al* (2007), symbols show their measurements of σ_D (squares) and σ_i (rhombs), solid line and dashed line show σ_D and σ_i computed by Amromin (2014).

The impact of water tunnel walls was taken into account during computation of the inviscid part of flow. The effect of surface tension on the cavity shape in the vicinity of X_1 is also taken into account in MZM model (unlikely to computations with MVD models). On the other hand, the cavity content was not considered in the versions of MZM employed for prediction of cavitation inception.

The predictions presented in Figure 13 relate to the Reynolds number effect on cavitation inception for the body already considered in Figures 2,5,7. The computational results were obtained using the viscous-inviscid interaction procedure for MZM model (the corresponding algorithm was described by Amromin (2021) in more detail). The experimental data were obtained by Katz (1984), Holl and Billet (1981), and Gorshkov and Kalashnikov (1970) in various facilities.

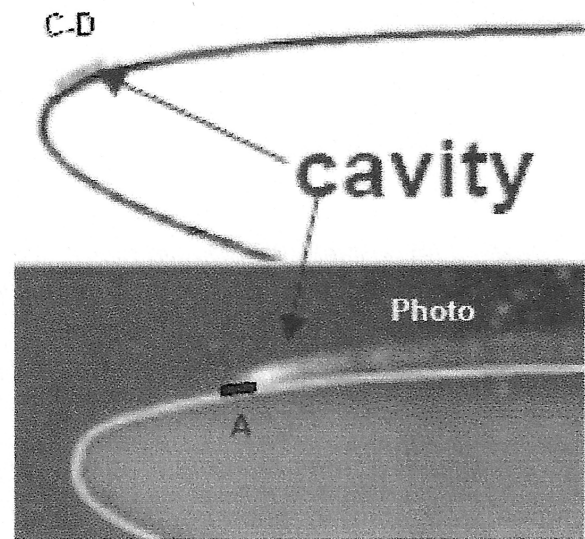


Figure 12. Cavity shapes and locations computed by Amromin (A, in the bottom) and by Coutier-Delgosha *et al* (C-D, in the top) superimposed on their photo.

The gradual increase of cavitation inception and desinence numbers with an increase of Re is seen in Figure 13. However, Arakeri and Acosta (1976) obtained another trend $\sigma_i(Re)$ for the same body with a trip installed on its nose for enhancing laminar-turbulent transition. Relaminarization of boundary layer behind the trip took place in their experiment at $Re < 4 \times 10^5$. As shown in Figure 14, $\sigma_i(Re)$ goes down for greater Re in their experiment and Amromin (2021) computations captured this trend. So, the significant effect of laminar-turbulent transition on inception of sheet cavitation can be predicted.

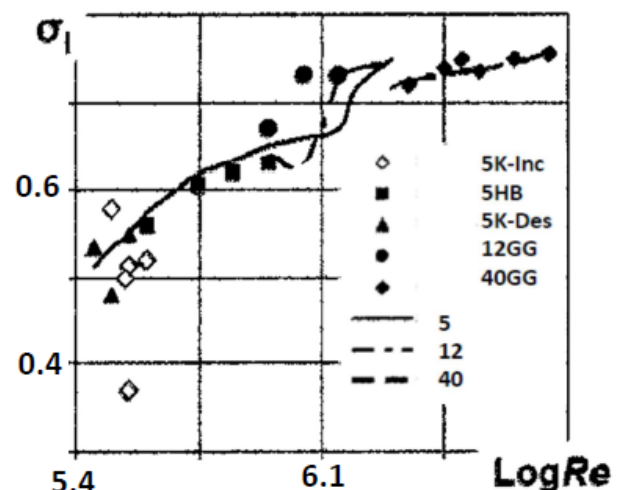


Figure 13. Cavitation inception and desinence numbers for bodies with hemispherical heads; symbols for experimental data from Holl and Billet on σ_i are marked as 5HB, for data from Gorshkov and Kalashnikov on σ_D as 12GG and 40GG, for data from Katz as 5K. Number at symbols and at Amromin's computational curves show values of D (in cm).

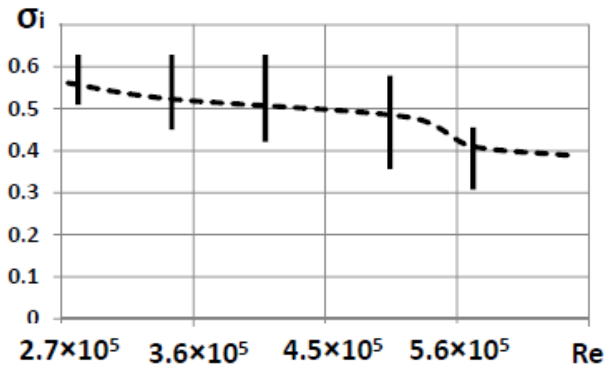


Figure 14. Computed dependency $\sigma_i(Re)$ for the body with hemispherical head with trip (curve) and observed value of this body (segments).

As mentioned above, comparisons of computed results with the experimental data have been affected by the difference $d\sigma = \sigma - \sigma_{vapor}$. As noted by Arndt *et al* (1979), this difference is proportional to a/U_0^2 . As pointed out by Kabayashi *et al* (2021), this difference is bigger for smaller cavities. The effect of the Amromin (2016) correction to σ_{vapor} on comparison of his computational results with the experimental data of Arakeri and Acosta (1976) for the same body without the trip is shown in Figure 15.

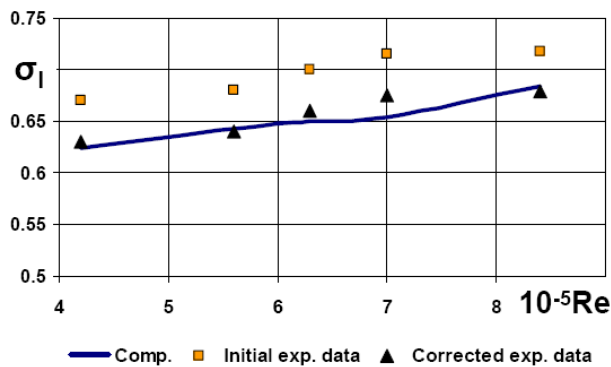


Figure 15. Computed and measured cavitation inception numbers for a body with hemispherical head.

The improvement of agreement of theory and experiment is clearly seen there. A similar improvement due to this correction is shown in Figure 16 for the hydrofoil NACA16012 tested by van Meulen (1980). Fluid-structure interaction also influences cavitation inception and desinence, as it is shown in Figure 17 with the results of Amromin (2017). Generalization of this version of MZM model for marine propeller blades cavitation was also successful, as manifested by Amromin *et al* (1995). Meanwhile, it is necessary to note that usually the inflow for them is not curl-free because of the hull wakes and such an inflow must be determined outside of MZM model. Also, pattern of small partial cavities could be successfully determined with MVD models (like done by Bensow and Bark (2010); but they did not study cavitation inception).

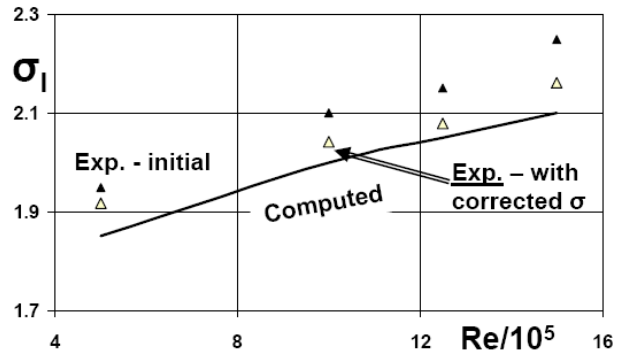


Figure 16. Effect of correction for σ on agreement of computed and measured cavitation inception number for hydrofoil NACA 16012 at 6° angle of attack.

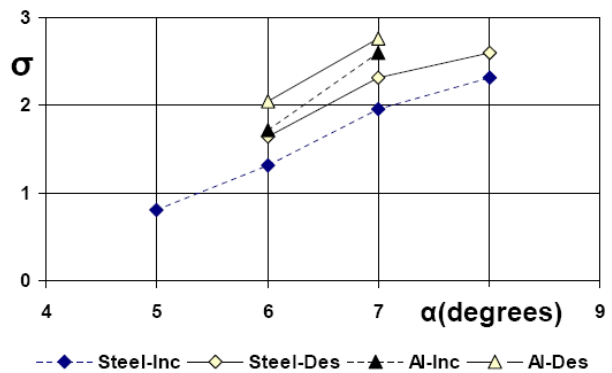


Figure 17. Cavitation inception and desinence numbers for aluminium and steel Cav2003.

4. CAVITATION INCEPTION IN VORTEXES

Meanwhile, cavitation of marine propellers frequently starts in tip vortexes. McCormick (1962) combined his pioneer experimental study of tip vortex cavitation with the attempt to find a single trend for the dependency $\sigma_i(Re)$. However, as one can see in Figure 18 plotted with his experimental data, there are very different trends for greater

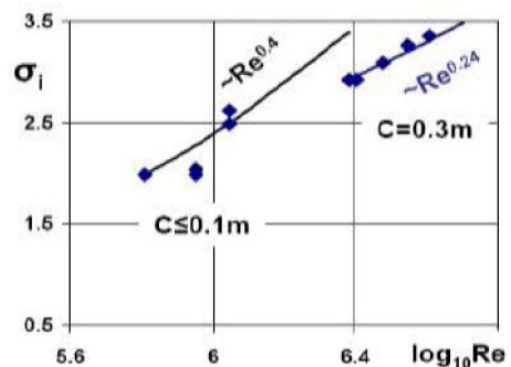


Figure 18. Approximations (solid lines) of the experimental data (rhombi) for hydrofoil tip vortex cavitation inception.

Re and for smaller Re . His attempt has been unsuccessfully revived by numerous researchers, but finally it became clear that the trend difference is caused by the difference in the kinds of boundary layers around the tip vortexes in the different ranges of Re . So, usually full-scale vortex cavitation cannot be predicted by scaling the results of the tests of small size model. Hsiao and Chahine (2008) captured the high- Re trend with their original multi-zone computational model of vortex cavitation in turbulent flow and found that $\sigma_i \sim Re^{0.23}$.

Meanwhile, as seen in Figure 19 with the results of Savio *et al* (2008), the well-known MVD solvers are unable to satisfactory predict vortex cavitation inception. Some more recent MVD studies of vortex cavitation did not compare their results with experiments (like Chen *et al* (2019), f. e.) and cannot be evaluated.

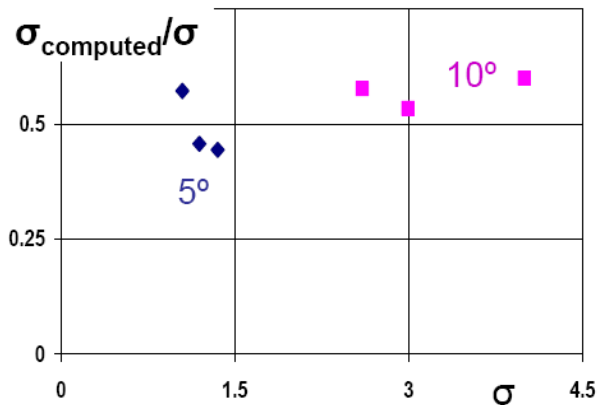


Figure 19. Ratio of computed with ANSYS RANS and measured by tip vortex cavitation inception numbers for two values of the angle of attack α at $Re \sim 10^6$

The substantial specific of vortex cavitation neglected in the majority of its studies is in the particular velocity profile in the vortex viscous core in turbulent flows. It is different from broadly used Rankine (laminar) profile. As derived by Amromin (2007) from Reynolds equation written in polar coordinates with the assumption about insignificant variations of $\langle u'v' \rangle$ around the vortex axis, this profile is

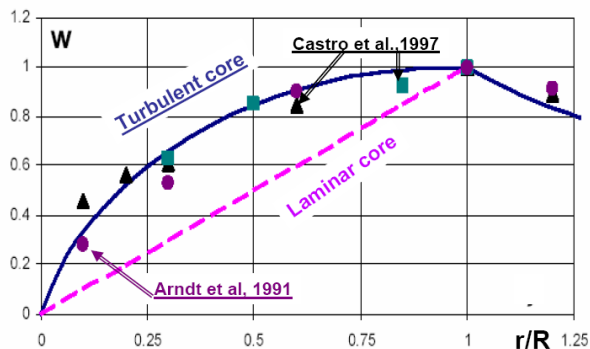


Figure 20. Theoretical (curves) and measured (symbols) velocities in vortex cores.

$$w(r) = (1 - \ln|r/R|)r/R \quad (1)$$

Here the radius r is counter from the vortex axis, $R = \sqrt{\Gamma \nu} / \sqrt{-\pi \langle u'v' \rangle}$. Comparison of Eq. (1) with the experimental data of Arndt *et al* (1991), Castro *et al* (1997) and with the velocity in the laminar core in Figure 20 manifests the incomparably better agreement of Eq. (1) with experimental data.

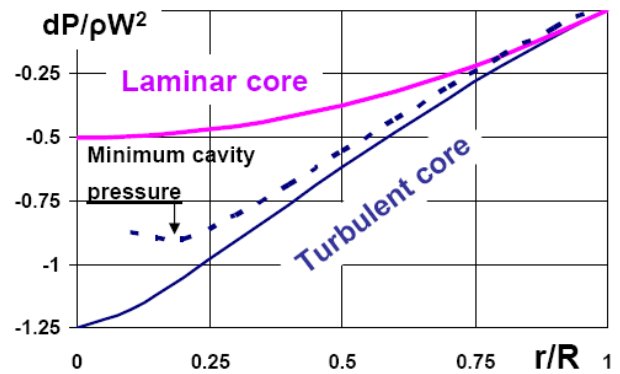


Figure 21. Comparison of the pressure drop within laminar and turbulent cavitation-free vortex cores (solid lines) and within a cavity of the radius r in turbulent core (dashed line); $dP = P(r) - P(R)$.

A cavity in the vortex core appears as a chain of bubbles. Therefore, the corresponding value of cavitation inception number depends on the bubble radius R_c as

$$\sigma_i = \left[\left(\frac{\langle u'v' \rangle}{2\nu} \right)^2 R_c R - \frac{4\chi}{\rho_w R_c} \right] U^{-2} - C_p \quad (2)$$

R_c must deliver a minimum for the right-hand side of Eq. (2). As shown in Figure 21, such a minimum exists at $R_c > 0$. The employment of Eq. (2) allowed for the significant improvement of the agreement of prediction of vortex

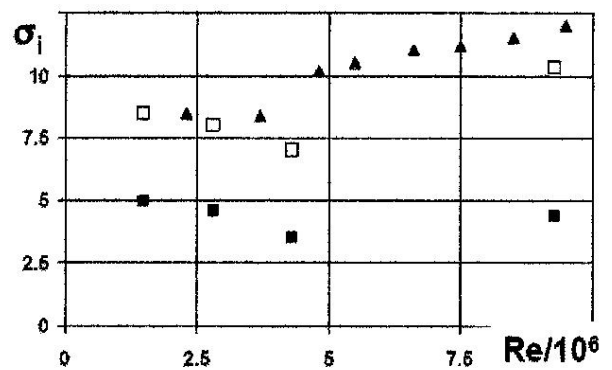


Figure 22. Comparison of experimental data for vortex cavitation behind a propeller blade (triangles) with computations carried out with using Rankine core (filled squares) for determination of vortex pressure and using Eq.(2) for its determination (empty squares).

cavitation inception with experimental data of Chesnakas and Jessup (2003), as was proven by Agrawal (2010) and can be seen in Figure 22 along with the results obtained using Rankine vortex core.

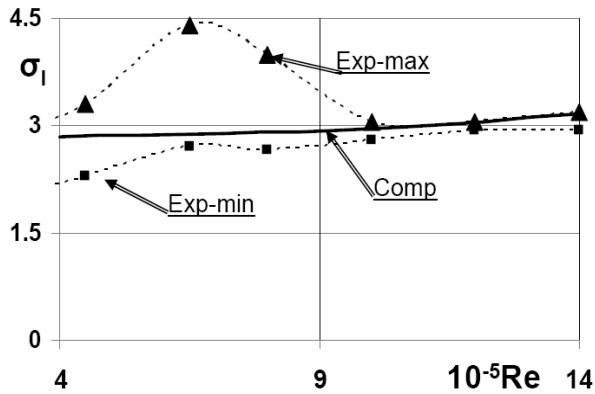


Figure 23. Cavitation inception numbers versus Reynolds number for disks.

The same Eq. (2) was used for determination of cavitation inception numbers behind blunt bodies. An example of this was provided by Amromin (2019) in comparison with Arndt (1978) experimental data is shown in Figure 23. However, it is necessary to point out that integral relationships employed to obtain the presented numerical results cannot provide values of Γ and $\langle u'v' \rangle$. These values were obtained using some approximations of known data for suitable flows. However, contemporary solvers for turbulent flows could be also used for this.

5. CAVITATION INCEPTION BEHIND SURFACE IRREGULARITIES

The above-considered flows take place around bodies of smooth surfaces. The practically important problem of prediction of cavitation inception behind surface irregularities has not been popular in computational studies of cavitation. Cavities near irregularities mounted over surfaces appear in vortexes drifting in separation zones created by irregularities themselves (like in the flow sketch in Figure 24).

The velocity profile (1) is also applicable to these vortexes. The mentioned viscous-inviscid interaction

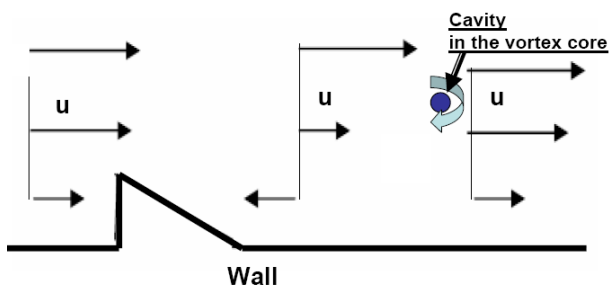


Figure 24. Sketch of flow with vortex cavitation behind a surface irregularity.

procedure can be also applied to computation there. However, the inflows for them are not uniform and it is not curl-free (this situation is similar to existing for marine propeller blades). Nevertheless, an account of the inverse influence of variations of separation zone thickness on pressure distribution along it can be carried out using a potential of velocity perturbations, as was already used by Amromin (2016, 2019). This computational procedure was used for the example of cavitation behind solitary irregularities in 2D flows presented in Figure 6 (for ridges tested by Arndt *et al* (1979)), in Figure 25 (for a small backward facing step tested by Katz (1984)), in Figures 26 and 27 (for triangles tested by Arndt *et al* (1979) and by Holl *et al* (1986)). The mentioned correction on inflow air content was used in preparation of Figure 26.

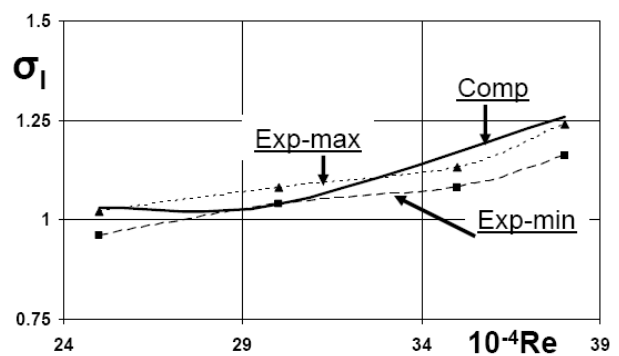


Figure 25. Comparison of computed cavitation inception numbers with measurements for a body with a backward step behind the hemispherical head.

Computations for slots and other irregularities located below the wall level have been carried out with taking into account that for the ratio of slot length to its depth $L/H \sim 1$, the slot bottom vicinity has a little influence on the other parts of flow (and these parts even were excluded from the measurements of Liu and Katz (2008)).

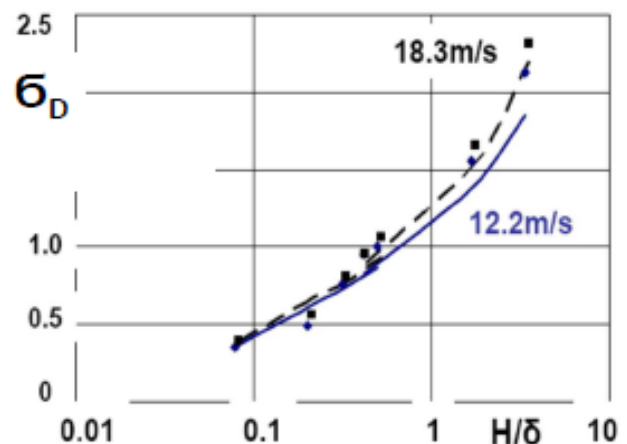


Figure 26. Computed (lines) and measured by (symbols) cavitation desinence numbers for triangles in flows without pressure gradient. Number at curves show U_0 values.

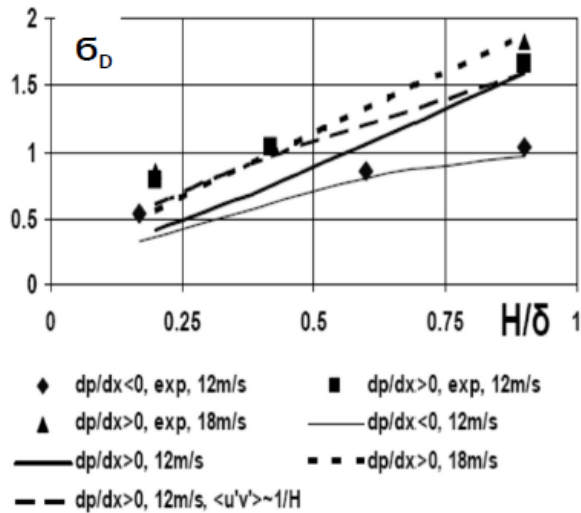


Figure 27. Effect of pressure gradient on cavitation desinenence numbers for triangles. Computed dependencies for various U_0 are shown by lines, experimental data—by symbols.

On the other hand, cavities in slots appear in vortices of the relatively stable location near the trailing edge of the slop. Examples of comparison of computed by Amromin (2019) results for cavitation inception in slots with the experimental data of Liu and Katz (2008) are provided in Figures 28. The computed results in these figures (as well as in Figure 6) were obtained for the initially selected values of R_c that do not provide the maxima of the right-hand side of Eq. (2). One can see there that the value of R_c significantly affects such results. Also, the impact of inflow gas content is emphasized in Figure 28. Explanation of the physics of this impact remains to be a challenge. The

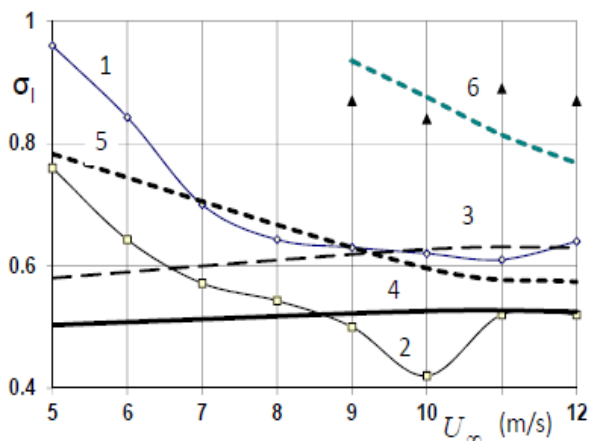


Figure 28. Comparison of computed and observed cavitation inception number for slots. Lines 1 and 2 provides maximum and minimum of observed σ_1 for the basic level of dissolved oxygen, triangles show average σ_1 for fivefold higher oxygen level. Line 3 shows computed σ_1 for $R_c=0.1\text{mm}$, line 4 –for 0.15mm . Line 5 shows $\sigma_1+d\sigma$ fitted to the basic oxygen level using line 4, line 6 shows $\sigma_1+d\sigma$ recalculated from line 4 for fivefold its level.

authors of many studies have tried to explain the inflow air content effects on the cavity expansion by consideration of air diffusion to the cavities. However, the differences of their predictions with the experimental data were too high (with data of Yu and Ceccio (1997), it was more than 4 times).

On the other hand, Amromin (2018a) tried to explain this expansion considering the bubble drift from liquid to the cavity surfaces under impact of the pressure gradient. Comparison of his estimate of air entrainment by cavities with the measurements of Lee *et al* (2016)] in Figure 29 looks satisfactory, but there is the necessity in the additional experimental proofs for such an explanation.

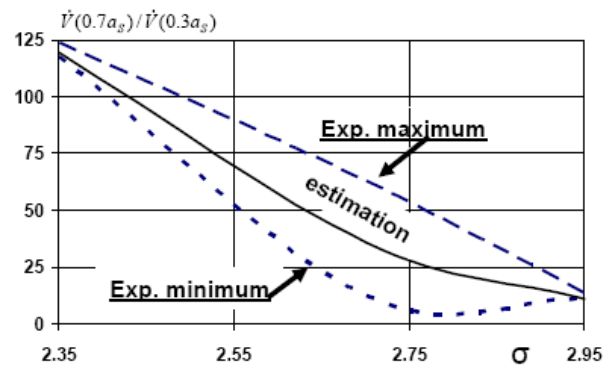


Figure 29. Impact of inflow air content on the ratio of air entrainments by a partial cavity.

There are also other unresolved issues for predictions of cavitation inception in full-scale conditions. One of practically important situation with cavitation over distributed surface irregularities is associated with the blade biofouling (as one can find more detail in the paper by Sezen *et al* (2021) in particular). Computations for cavitation inception over the walls with distributed surface irregularities are more complex.

$$u(y) = v^* \left[\ln \left| \frac{(y + y_0) v^* / \nu}{\kappa + B} \right| \right] \quad (3)$$

The velocity along the wall is also linked to the friction velocity v^* , but the coefficients B and y_0 depend on the parameter $\Lambda = HU^{-1}dU/dx$ there. Besides, the sizes and distributions of irregularities are not uniform. So, now this problem is not solved and seems to be too difficult even for formulation.

6. THE NEXT STEPS FOR FULL SCALE FLOWS

Predictions of cavitation inception in marine engineering are aimed on full-scale flows that significantly differ from the flows in the testing facilities. Inventions in model tests may reduce this difference. For example, it is possible to increase cavitation inception number up to its full-scale value by seeding additional cavitation nuclei in the inflow of the water tunnel, as was described in the compendium

edited by Dern *et al* (2015); however, there will be an issue of determination of seeding concentration. Moreover, the water tunnel flows have the specific features that are not typical for the full-scale ship flows, as patch cavitation analysed by Amromin (2020). So, some employment of computational tools for prediction of cavitation inception is rather unavoidable. Here it is appropriate to recall that for diverse kinds and stages of cavitation the diverse flow models and computational tools are suitable. For supercavitation, the body surface and boundary layer characteristics are secondary, whereas the cavity content may be important. The situation is opposite for determination of cavitation inception.

The presented achievements in prediction of cavitation inception were obtained mainly using MZM. Let us point out that the used multi-zone model includes up to 8 diverse zones along viscous part of the flow and up to 3 free surfaces along the boundary of inviscid flow. However, the described MZM results were obtained with viscous-inviscid interaction methods employing integral boundary layer equations. It would not be realistic to expect an extensive spread and amelioration of such methods in the near future.

It would be more realistic to seek modifications of existing RANS or LES solvers to allow for the multi-zone analysis of cavitation and for the more accurate analysis of its effects. The important issue relates to the use of such solvers is that flow in the vicinity of wall in separation zones does not yield to Eq. (3). The wall functions in these zones would be better defined with the use of Simpson *et al* (1981) experimental data for separated flows, but there is no hope to take such functions from the solvers for fully turbulent flows because, as pointed out by Raiesi *et al* (2011) and Liedrand *et al* (2021), these solvers were tuned with the data sets for separation-free one-phase flows. Also, there is no hope to obtain such wall functions from DNS because, as emphasized by Barenblat *et al* (2014), nothing substantial in turbulence theory was derived directly from Navier-Stokes equations.

The most promising path of prediction of cavitation inception over complex shape bodies and ship elements in the high-Re 3D flows is to combine the multi-zone multi-scale quasi-2D analysis of incipient cavitation with employment of existing RANS or LES solvers for cavitation-free flows. Their employment should be considered as determination of the unperturbed initial (unperturbed) approaches for the following determination of characteristics of cavitation-induced perturbations using MZM methods. Such an employment would be similar to the use of a BEM method as the initial approach by Amromin *et al* (1990, 1995), but RANS or LES unperturbed approach would give a more accurate unperturbed results because of an account of viscous effects on hydrodynamic loads. Fortunately, these loads

and streamlines upstream the cavities are insignificantly affected by incipient cavitation. Therefore, quasi-2D MZM methods can be employed then for determination of relatively small cavity-induced perturbations and cavitation inception numbers.

It is also important to pay more attention to validation of the developed solvers. In particular, the frequent use of experimental data of Rouse and McNown (1948) obtained at $Re < 3 \times 10^5$ for validation of solvers developed for fully turbulent flows looks as a paradox. Validation for full-scale condition is a hard task because usually the sea test of one ship gives one experimental point only, whereas the measurement discrepancy can be quite high (one can see Vriidag (2009), f. e.).

Finally, cavitation inception in full-scale conditions is basically a random phenomenon. Its randomness takes place not only because of the substantially stochastic nature of full-scale turbulent flows (perfectly emphasized by Harsha (1977) many decades ago). The ocean environment is always substantially stochastic due to the impact of waves. It would be desirable to operate with mathematical expectancies of characteristics of cavitation, but such an approach does not exist yet.

7. CONCLUSIONS

Cavitation inception is a complex phenomenon because it appears on ship elements and their models in various forms and it is affected by various physical factors. Some of them substantially complicate extrapolations of the model test outcomes to the full-scale conditions. This complication amplifies the importance of computational analysis of cavitation inception.

Such an analysis was too difficult for classical mathematical methods, but the contemporary development of theoretical models and computational tools made it possible to predict cavitation inception numbers at least for the forms most usual for both full scale and model test conditions. The more successful predictions were achieved with employment of multi-zone model of cavitation (MZM) and with the solution for velocity in the vortex core in turbulent flows. The achievements in predictions for sheet cavitation of smooth hydrofoils, bodies and for cavitation behind various surface irregularities are presented in this paper with the explanation of the employed computational models, whereas readers are addressed to already published papers for more detail on the employed algorithms.

On the other hand, employed in MZM computational tools are insufficient for studying complex 3D flows. The most promising paths of employment of the developed models to 3D flows and the opportunities of a combined employment of MZM models with contemporary CFD solvers for fully turbulent cavitation-free flows.

8. REFERENCES

1. ACOSTA, A.J., PARKIN, B.R. (1975) *Cavitation Inception. A Selective Review*. J. Ship Research 19: 193-205
2. AGARWAL, A. (2010) *Analysis of vortex cores in turbulent flows*. J. Turbulence 11: 1-9
3. AHUJA, V., HOSANGADI, A. and S. ARUNAIATESAN, S. (2001) *Simulation of Cavitating Flows Using Hybrid Unstructured Meshes*. ASME J. Fluids Eng.- 123: 331-338
4. AMROMIN, E.L. (1985) *On cavitation flow calculation for viscous capillary fluid*. Fluids Dynamics - 20: 891— 897
5. AMROMIN, E.L. (2007) *Analysis of vortex core in steady turbulent flow*. Phys. Fluids - 19: 118108
6. AMROMIN, E. L. (2014) *Development and validation of CFD models for initial stages of cavitation*. ASME J. Fluids Eng. 136: 081303
7. AMROMIN, E.L. (2016) *Analysis of cavitation inception and desinence behind surface irregularities*. Ph. Fluids 28: 075106
8. AMROMIN, E.L. (2017) *Impact of hydrofoil material on its cavitation inception and desinence*. ASME J. Fluids Eng. 139: 061304
9. AMROMIN, E.L. (2018) *Prediction of cavitation inception within regions of flow separation*. ASME J. Fluids Eng. 140: 011103
10. AMROMIN, E.L. (2018a) *Explanation of the influence of inflow air content on the lift of cavitating hydrofoils*. ASME J. Fluids Eng. 140: 084501
11. AMROMIN, E.L. (2019) *Prediction of cavitation inception in slots*. Int. J. Multiphase Flows - 119: 217-222
12. AMROMIN, E.L. (2020) *The origin of patch cavitation*. Int. J. Multiphase Flows -124: 103188
13. AMROMIN, E.L. (2021) *Modeling of the impact of laminar-turbulent transition on cavitation inception*. Applied Ocean Res. 114: 102796
14. AMROMIN, E.L., MISHKEVICH, V.G., ROZHDESTVENSKII, K.V. (1990) *Approximate Calculation of Three- Dimensional Cavitating Flow around Marine Propeller Blade in Viscous Capillary Fluid*. Fluid Dynamics 25: 879-885
15. AMROMIN, E.L., VACILIEV, A.V., SYRKIN, E.N. (1995) *Propeller Blade Cavitation Inception Prediction and Problems of Blade Geometry Optimization: Recent Research at the Krylov Shipbuilding Research Institute*. J. Ship Res. 39: 202-212
16. ARAKERI, V.H. (1975) *Viscous effects on the position of cavitation separation from smooth bodies*. J. Fluid Mech. 68: 779-799
17. ARAKERI, V.H., ACOSTA, A.J. (1976) *Cavitation inception observation on axisymmetric bodies at supercritical Reynolds numbers*. J. Ship Res. 20: 40-50
18. ARNDT, R.E.A. (1978) *Investigation of the effect of dissolved gas and free nuclei on cavitation and noise in the wake of a sharp edge disk*. Joint IAHR/ASME/ASCE Symp. Design and Operation of Fluid Machinery, Fort Collins., Colorado- II: 543-555
19. ARNDT, R.E.A., ARAKERI, V.H., HIGUCHI, H. (1991) *Some observations of tip-vortex cavitation*. J. Fluid Mech. 229: 269-289
20. ARNDT, R.E.A., HOLL, J.W., BOHN, J.C. & BECHTEL, W.T. (1979) *Influence of surface irregularities on cavitation performance*. J. Ship Res. 23: 150-170
21. ARNDT, R. E. A., KELLER, A. P. (1992) *Water Quality Effects on Cavitation Inception in a Trailing Vortex*. ASME J. Fluids Eng.114: 430-438
22. BARENBLATT, G.I., CHORIN, A.J., PROSTOKISHIN, V.M. (2014) *Turbulent flows at very large Reynolds numbers: Lessons learned*. Phys. Uspekhi 57: 265-272
23. BENSON, R.B., BARK, G. (2010) *Implicit LES Predictions of the Cavitating Flow on a Propeller*. ASME J. of Fluids Eng. 132: 041302
24. BIRKHOFF, G. (1971) *Mathematical Analysis of Cavitation*. UITAM Symp. High-Speed Flows, Leningrad
25. BLAKE, W.K. (1986) *Mechanics of Flow-Induced Sound and Vibration*. Academic Press, NY
26. CASTRO, E., CRESPO, A., MANUEL, F. and FRUMAN, D.H.J. (1997) *Equilibrium of Ventilated Cavities in Tip Vortices*. ASME J. Fluids Eng. 119: 759-767
27. CAUPIN, F., HERBERT, E. (2006) *Cavitation in water: a review*. Comp. R. Physique 7: 1000–1017
28. CECCIO, S.L., BRENNEN, C.E. (1992) *Dynamics of sheet cavities on bodies of revolution*. ASME J. Fluids Eng. 114: 93-99
29. CHEN, L., ZHANG, L., PENG, X., SHAO, X. (2019) *Influence of water quality on the tip vortex cavitation inception*. Phys. Fluids 31: 023303
30. CHESNAKAS, C. J. and JESSUP, C. D. (2003) *Tip-vortex induced cavitation on a ducted propulsor*. ASME Paper FEDSM 2003–45320
31. COUTIER-DELGOSHA, O., DENISET, F., ASTOLFI, J.A. and LEROUX, J-B. (2007) *Numerical Prediction of Cavitating Flow on a Two-Dimensional Symmetrical Hydrofoil and Comparison to Experiments*. ASME J. Fluids Eng. 129: 279-292
32. DERN, J-C., QUENEZ, J-M., WILLSON, P. (2015) *Compendium on naval hydrodynamics*. Paris, ENSTA
33. GANESH, H., MAKIHARJU, S.A., CECCIO, S.L. (2016) *Bubbly shock propagation as a mechanism for sheet-to-cloud transition of partial cavities*. J. Fluid Mech. 802: 37-78

34. GONSALES, E., PATELLA, R.F. (2009) *Numerical Simulation of Cavitating Flows with Homogeneous Models*. Computers and Fluids - 38: 1682-1696
35. GORSHKOV, A.S. and KALASHNIKOV, Y.N. (1970) *The scale effect on incipient stage of cavitation on body of revolution*. Trans. Krylov Ship Res. Institute, #258, 1970 (in Russian)
36. HARSHA, P.T. (1977) *Kinetic Energy Methods*. Handbook of Turbulence 1: 187-236, Plenum, NY
37. HOLL, J.W., BILLET, M.L. (1981) *Scale effects on various types of limited cavitation*. ASME J. Fluids Eng. 103: 405-414
38. HOLL, J.W., BILLET, M.L., TADA, M. and STINEBRING, D.R. (1986) *The Influence of Pressure Gradient on Desinent Cavitation from Isolated Surface Protrusions*. ASME J. Fluids Eng. 108: 254-260
39. HSIAO, C-T. and CHAHINE, G. L. (2008) *Scaling of Tip Vortex Cavitation Inception for a Marine Open Propeller*. 27th Symp. Naval Hydrodynamics, Seoul
40. IVANOV, A.N. (1980) *Hydrodynamics of developed cavitating flows*. Sydstroenie, Leningrad (in Russian)
41. KATZ, J. (1984) *Cavitation phenomena within regions of flow separation*. J. Fluid Mech. 140: 397-436
42. KOBAYASHI, K., KATAYAMA, Y., WATANABE, S., Tsuda, S. (2021) *Experimental Investigation on Cavity Pressure Inside Sheet Cavitation*. ASME J. Fluids Eng. 143: 121102
43. KOPRIVA, J., AMROMIN, E.L., ARNDT, R.E.A. (2008) *Improvement of Hydrofoil Performance by Partial Ventilated Cavitation in Steady Flow and Periodic Gusts*. ASME J. Fluids Eng. 130: 03130
44. KUNZ, R.F, BOGER, D.A., STINEBRING, D.R., CHYCZEWSKI, T.S., LINDAU, J.W., GIBELING, H.J., VENKATEAWAREN, S. and GOVINDAN, T.R. (2000) *A preconditioned Navier-Stokes method for two-phase flows with application to cavitation prediction*. Computers and Fluids 29: 849-875
45. LEE, I-H., MAKIHARJU, S.A., GANESH, H. and CECCIO, S.L. (2016) *Scaling of Gas Diffusion into Limited Partial Cavities*. ASME J. Fluids Eng. 138: 051301
46. LIEDRAND, R., KLAPWIJK, M., LLOYD, T., VAZ, G. (2021) *Transition and Turbulence Modeling for the Prediction of Cavitating Tip Vortices*. ASME J. Fluids Eng. 143: 011202
47. LINDGREN, H. and JOHNSON, C. A. (1966) *Cavitation inception on head form ITTC: Comparative experiments*. 14th ITTC conf. Tokyo
48. LIU, X. and KATZ, J. (2008) *Cavitation phenomena occurring due to interaction of shear layer vortices with the trailing corner of a two-dimensional open cavity*. Phys Fluids 20: 041702
49. McCORMICK, B.W. (1962) *On cavitation produced by a vortex trailing from a lifting surface*. J. Basic Eng. 84: 369-386
50. MEULEN, J.H.J. van der (1980) *Boundary layer and Cavitation Study of NACA16012 and NACA4412 hydrofoils*. 13^{en} Symp. Naval Hydrodyn., Tokio
51. PELONE, C. and ROWE, A. (1988) *Effect of separation on partial cavitation*. ASME J. Fluids Eng. 110: 182-189
52. RAIESI, H., PIOMELLI, U. and POLLARD, A. (2011) *Evaluation of turbulence models using direct numerical and large-eddy simulation data*. ASME J. Fluids Eng. 133: 021203
53. ROUSE, H. and McNOWN, J.S. (1948) *Cavitation and Pressure Distribution: Head Forms at Zero Angle of Yaw*. State Univ. Iowa, bul. 32. Iowa City
54. SAVIO, L., PITTALUGA, C., VIVIANI, M., FERRANDO, M. and CONTI, F. (2008) *An experimental and numerical study of cavitation on hull appendages*. Conf. on High. Performance Marine Vehicles, Naples
55. SEZEN, S., UZUN, D., OZYURT, R., TURAN, O. ATLAR, M. (2021) *Effect of biofouling roughness on a marine propeller's performance including cavitation and underwater radiated noise (URN)*. Applied Ocean Res. 107: 102491
56. SIMPSON, R.L., CHEW, Y-T. and SHIVAPRASAD, B.G. (1981) *The structure of a separating turbulent boundary layer. Part 1. Mean flow and Reynolds stresses*. J. Fluid Mech. 113: 23-51
57. SINGHAL, A.K., ATHAVALE, M.M., LI, H. & JIANG, Y. (2002) *Mathematical Basis and Validation of the Full Cavitation Model*. ASME J. Fluids Eng. 124: 617-624
58. ULHMAN, J.S. (1987) *The surface singularity method applied to partially cavitating hydrofoil*. J. Ship Res. 31: 107-124
59. VRIIDAG A. (2009) *Control of propeller cavitation in operational conditions*. PhD thesis TU Delft.
60. WADE, R.B., ACOSTA, A.J. (1966) *Experimental observation of the flow past a plano-convex hydrofoil*. ASME J. Basic Eng. 88: 273-283
61. WANIEWSKI, T.A., BRENNEN, C.E. (1999) *The Evolution of Cavitation Events with Speed and Scale of the Flow*. ASME paper FEDSM99-7916
62. YU, P-W., CECCIO, S.L. (1997) *Diffusion Induced Bubble Population Downstream of a Partial Cavity*. ASME J. Fluids Eng. 119: 782-787
63. ZHANG, G., KHILFA, I., COUTIER-DELGOSHA, O. (2020) *A comparative study of quasi-stable sheet cavities at different stages based on fast synchrotron x-ray imaging*. Ph. Fluids 32: 123316